ADVANCED MATERIALS
www.advmat.de

Overcoming Barriers Associated with Oral Delivery of Differently Sized Fluorescent Core-Shell Silica Nanoparticles

*Jacob A. Erstling, Nirmalya Bag, Thomas C. Gardinier, Ferdinand F. E. Kohle, Naedum DomNwachukwu, Scott D. Butler, Teresa Kao, Kai Ma, Melik Z. Turker, Grant B. Feuer, Rachel Lee, Nada Naguib, James F. Tallman, Henry F. Malarkey, Lieihn Tsaur, William L. Moore, Dana V. Chapman, Tangi Aubert, Saurabh Mehta, Richard A. Cerione, Robert S. Weiss, Barbara A. Baird, and Ulrich B. Wiesner**

Oral delivery, while a highly desirable form of nanoparticle-drug administration, is limited by challenges associated with overcoming several biological barriers. Here, the authors study how fluorescent and poly(ethylene glycol)-coated (PEGylated) core-shell silica nanoparticles sized 5 to 50 nm interact with major barriers including intestinal mucus, intestinal epithelium, and stomach acid. From imaging fluorescence correlation spectroscopy studies using quasi-total internal reflection fluorescence microscopy, diffusion of nanoparticles through highly scattering mucus is progressively hindered above a critical hydrodynamic size around 20 nm. By studying Caco-2 cell monolayers mimicking the intestinal epithelia, it is observed that ultrasmall nanoparticles below 10 nm diameter (Cornell prime dots, [C' dots]) show permeabilities correlated with high absorption in humans from primarily enhanced passive passage through tight junctions. Particles above 20 nm diameter exclusively show active transport through cells. After establishing C' dot stability in artificial gastric juice, in vivo oral gavage experiments in mice demonstrate successful passage through the body followed by renal clearance without protein corona formation. Results suggest C' dots as viable candidates for oral administration to patients with a proven pathway towards clinical translation and may generate renewed interest in examining silica as a food additive and its effects on nutrition and health.

1. Introduction

The route of administration of therapeutic drugs to patients plays a significant role in patient disease outcomes. Oral administration is typically associated with higher patient adherence and an enhanced capability for repeat dosing when compared to intravenous administration.[1–6] The last two decades have seen substantial efforts in nanoparticle-based drug delivery.[7–11] In contrast to small molecule therapeutics, the oral delivery of nanoparticles has been significantly hindered by the fact that most nanoparticle platforms are not effectively absorbed through the gastrointestinal (GI) tract into the bloodstream.[12] In addition to surviving stomach acid, any orally delivered therapeutic must overcome two major barriers in the GI tract: the dense mucosal layer covering the epithelial lining as well as the epithelial lining itself (**Figure 1**).[13] In this work, we study fluorescent

J. A. Erstling[+], T. C. Gardinier[+], F. F. E. Kohle, T. Kao, K. Ma[+++], M. Z. Turker[+], R. Lee, N. Naguib, J. F. Tallman, L. Tsaur, W. L. Moore, D. V. Chapman[++++], T. Aubert[+++++], U. B. Wiesner
Department of Materials Science and Engineering
Cornell University
Ithaca, NY 14853, USA
E-mail: ubw1@cornell.edu

The ORCID identification number(s) for the author(s) of this article can be found under https://doi.org/10.1002/adma.202305937

[+]Present address: Elucida Oncology, 1 Deer Park Drive, Suite E Monmouth Junction, NJ 08852, USA

[++]Present address: Department of Chemistry, Indian Institute of Technology Kharagpur, Kharagpur, West Bengal 721302, India

[+++]Present address: Department of Biomedical Engineering, Tsinghua University, Beijing 100084, China

[++++]Present address: Department of Biomedical Engineering, Yale University, New Haven, CT 06511, USA

[+++++]Present address: ICGM, CNRS, ENSCM, University of Montpellier, Montpellier 34000, France

DOI: 10.1002/adma.202305937

J. A. Erstling[+], N. DomNwachukwu, G. B. Feuer, N. Naguib
Department of Biomedical Engineering
Cornell University
Ithaca, NY 14853, USA

N. Bag[++], F. F. E. Kohle, R. A. Cerione, B. A. Baird
Department of Chemistry and Chemical Biology
Cornell University
Ithaca, NY 14853, USA

S. D. Butler, R. S. Weiss
Department of Biomedical Sciences
Cornell University
Ithaca, NY 14853, USA

H. F. Malarkey
Department of Applied and Engineering Physics
Cornell University
Ithaca, NY 14853, USA

S. Mehta
Center for Precision Nutrition and Health
Division of Nutritional Sciences
Cornell University
Ithaca, NY 14853, USA

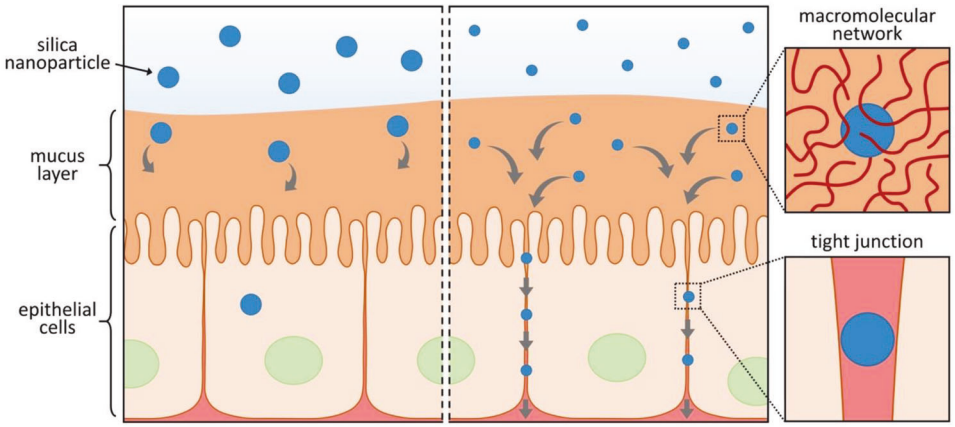

Figure 1. Schematic of two major barriers to oral delivery associated with the GI tract (not drawn to scale). The first barrier (top of figure) is the mucosal lining that inhibits free diffusion, for example, of nanoparticles (small round blue objects in the figure) as investigated here, restricting them from reaching the epithelial lining (enlarged box at top right shows an individual particle in blue surrounded by a macromolecular network in red constituting the mucus layer). The second barrier (bottom of figure) is the epithelial lining itself (individual cells shown with green cell nucleus) restricting the direct passage of nanoparticles through this layer. This barrier can be overcome by (left) active transport through a cell or by (right) passive transport through tight cell junctions (the enlarged box at the bottom right shows an individual particle in blue in a tight junction between two epithelial cells).

poly(ethylene glycol)-coated (PEGylated) core-shell silica nanoparticles with sizes systematically varied between 5–50 nm and their ability to overcome these barriers for oral delivery. To the best of our knowledge, in this size regime, careful studies elucidating the role of silica particle size in transport across these barriers – keeping all other parameters as constant as the synthesis allows – have not been reported before.

The mucus layer, composed of a heterogeneous mixture of diverse macromolecular protein and polysaccharide species, functions as a key barrier in the human body against disease and foreign objects such as nanoparticles.[14,15] Mucus constituents hinder the diffusion and permeability of foreign materials across the mucus layer via myriad interactions including electrostatic interactions, size-based exclusion, surface aggregation of proteins, and van der Waals interactions.[16,17] As fast-clearing mucus can trap these foreign objects and rapidly remove them from the body,[18,19] biophysical approaches have recently been used to evaluate nanoparticles of suitable size and surface characteristics that can diffuse through mucus barriers relatively rapidly.[20–22] While these studies considered physicochemical properties such as deformability and hydrophilic surface modification including PEGylation to facilitate nanoparticle diffusion through mucus, several key issues remained. Most work focused on particles greater than 100 nm in diameter which typically suffer from significant reticuloendothelial system (RES) uptake once absorbed by the bloodstream. This problem can be overcome by moving to ultrasmall nanoparticles (diameter < 10 nm) with hydrodynamic sizes below the cut-off for renal clearance.[23–27] Furthermore, inadequate time resolution of single particle tracking (SPT) experiments typically used for diffusion measurements of objects in mucus often make it challenging to quantify the relatively fast diffusion of smaller nanoparticles through this medium. SPT measurements are typically performed on a small number of particles, limiting data statistics and possibly resulting in insufficiently precise diffusion values.[28,29] While multiple particle tracking (MPT) methods can overcome the issue of limited dataset size, they may still suffer from inadequate time resolution.[30–32] Finally, these particle tracking measurements are often performed in freshly harvested mucus, making it difficult to replicate diffusion values due to day-to-day variations in mucus preparations.[28,30–32]

The epithelial lining acts as a second significant barrier and is primarily comprised of enterocytes that form tight junctions, rendering it a strong obstacle to the oral administration of nanoparticles (Figure 1).[33,34] A commonly utilized system to study the permeability of drugs and nanoparticles across the epithelial lining is the Transwell permeability assay.[35,36] This industry-standard test uses a human colorectal cancer Caco-2 cell line that forms a monolayer of cells with a structure similar to that of enterocytes, including the formation of tight junctions.[37,38] Enhanced permeability through a Caco-2 monolayer has been shown to correlate with higher uptake of compounds into the bloodstream when administered orally in human patients.[35,36,39] While prior studies demonstrated that decreasing nanoparticle size monotonically increased permeability across Caco-2 cell monolayers, few studies have focused on the ultrasmall (sub-10 nm diameter) size regime of nanoparticles.[40] Studies that have focused on ultrasmall nanoparticles, based primarily on metals (e.g., gold) or metal oxides (e.g., iron oxide), showed that they indeed exhibited increased permeability through Caco-2 cells and mouse intestines.[41–43] It is important to note, however, that none of the ultrasmall particles examined were based on silica. Since it is a first-of-its-kind investigational new drug (IND), Food and Drug Administration (FDA) approved human clinical trial established their safe use in humans,[25] ultrasmall silica nanoparticles have attracted considerable interest for diagnostic and

U. B. Wiesner
Kavli Institute at Cornell for Nanoscale Science
Cornell University
Ithaca, NY 14853, USA

therapeutic applications.[7] They are, therefore, also interesting subjects for investigations of their oral delivery capabilities.

Oral delivery studies of silica nanoparticles have revealed that particles with diameters > 20 nm are able to modulate the interactions between the tight junction protein ZO-1 and the actin cytoskeleton in Caco-2 cells.[44] While this effectively "opens" tight junctions, it does not create sufficiently large openings for these larger nanoparticles themselves to permeate the monolayer.[44–46] Silica nanoparticles have only been observed to cross Caco-2 layers when modified to contain highly charged species, cell-penetrating peptides, or zwitterionic coatings to promote their uptake into cells.[47,48] However, non-specific uptake as well as stability within the biological fluids of the GI tract and circulatory system are major concerns for these particles. Beyond these issues, the literature suggests that the major complications current silica nanoparticles face in oral delivery are complex synthesis and poor dispersity.[49] Our laboratory specializes in the development of ultrasmall and fluorescent silica core – PEG shell (core-shell) nanoparticles synthesized in aqueous solutions, termed Cornell prime dots (or C' dots), for biomedical applications.[25,50–52] The C' dot platform has been well characterized and shown to exhibit i) size control down to a single atomic silica layer through tuning of aqueous synthesis conditions,[50] ii) narrow particle size distribution (± 20% for 30 Å diameter silica core C' dots),[53] iii) dense surface coverage with a short (≈1 nm thick), brush-like PEG shell (only 6–9 ethylene oxide repeat units),[54] iv) homogenous surface chemical characteristics when employing positively charged dyes for encapsulation,[55,56] as well as v) versatile, stable, and quantifiable surface functionalizations.[57] In general, the surface chemistry of silica is very versatile and well-established. Surface conjugations performed with C' dots include up to 20–40 cancer drugs for therapeutic applications in oncology demonstrating a wide therapeutic index.[58–60] The large number of drugs on the C' dot surface leads to surprisingly high drug-loading capacities, for example, 1–2 orders of magnitude higher per vehicle volume than for antibodies (Abs) with their limited drug-to-vehicle ratios (typically around 5 drugs per Ab). Despite high drug-loading capacities, C' dots continue to show favorable biodistribution (BD) and pharmacokinetics (PK) profiles.[59,60] This has been ascribed to the insertion of the hydrophobic drugs in-between the brush-like PEG surface layer, lowering drug vehicle free energy in aqueous solutions and leaving the surface hydrophilic.[58] From extensive prior quantitative BD, PK, and toxicity studies in animals, as well as BD and PK studies in humans, it is now well established that their ultrasmall size allows intravenously injected C' dots to avoid substantial RES uptake while promoting renal clearance, a paradigm referred to as "target-or-clear".[25,26,61,62] As a result of these extensive safety studies and this favorable behavior, these particles are currently in both diagnostic and therapeutic human clinical trials (e.g., see clinicaltrials.gov identifiers: NCT01266096, NCT02106598, NCT04167969, and NCT05001282). This includes a folate receptor alpha (FRα) targeted and small molecule cytotoxic drug functionalized (i.e., exatecan, a topoisomerase 1 inhibitor) C' dot-drug-conjugate (CDC) that has now advanced to phase 2 human clinical studies.[58,59] Overall, their well-defined structural, compositional, and resulting favorable BD and PK characteristics already established in humans, which render them one of the most advanced nanomedicine-based organic-inorganic hybrid particle platforms in oncology, now make C' dots an interesting subject for fundamental studies of oral delivery.

In this work, we aim to investigate the ability of unfunctionalized (plain) fluorescent PEGylated core-shell silica nanoparticles with sizes systematically varied from ≈5 to 50 nm, that is, including, but not limited to, ultrasmall C' dots, to overcome the barriers associated with stomach acid, mucus, and epithelial lining, thereby assessing their potential for oral delivery as a function of particle size. Rather than immediately jumping into studies with highly toxic, drug-loaded silica nanoparticle vehicles, employing non-toxic materials substantially facilitates experimental work while still allowing baseline behavior of the plain particle platform to be established. Furthermore, we have recently discovered, to the best of our knowledge for the very first time for any nanoparticle, that ultrasmall plain C' dots can induce ferroptosis – a potent, highly specific, and unique form of cell death in cancer cell populations that are nutrient deprived – in the complete absence of a cytotoxic payload, and thus act as "self-therapeutic" agents in tumor-bearing mice.[51,63] Ferroptosis is induced, only in nutrient-deprived cells (i.e., cancer cells, not healthy cells), by iron, which is chelated by the C' dots via surface silanol groups, and transported into the cell.[51] In turn, it has recently been shown that cancer immunotherapies like immune checkpoint blockade (ICB) involve ferroptosis playing a cooperative role to achieve maximum efficacy.[64] Finally, we separately reported on particle-induced concomitant upregulation of the inflammatory cytokine genome and adaptive immune pathways, suggesting that the plain particle itself (without a drug) initiates distinct anti-tumoral immune responses in the tumor microenvironment.[65] All this suggests that oral delivery of the plain core-shell particle itself, that is, without cytotoxic drugs tethered to its surface, could already be valuable, for example, for combination therapies with immunotherapy.

To assess the potential of these base particles for oral delivery, we first show that imaging fluorescence correlation spectroscopy (imaging FCS), a total internal reflection fluorescence (TIRF) microscopy-based variant of FCS, can be used with excellent reproducibility and fidelity to study fluorescent nanoparticle diffusion through strongly scattering mucus.[66] The application of this technique substantially decreases the sample preparation and analysis time as compared to alternative methods of analysis. In these experiments, we observe a previously uncharacterized critical particle size around 20 nm, beyond which particle diffusion is progressively hindered in the mucus network relative to behavior in water. We then go on to examine particle size-dependent permeability across Caco-2 cell monolayers. Here too we demonstrate that particles above and below ≈10–20 nm in diameter exhibit qualitatively different behavior and that ultrasmall C' dots exhibit high enough permeability to be viable candidates for oral delivery in humans. In the final part of the study, we establish the stability of C' dots in gastric juice, which enables their direct oral administration in mice. By investigating the urine excreted by these animals at different time points following oral C' dot administration, we unambiguously demonstrate that the nanoparticles are renally cleared with essentially unaltered size, that is, no protein corona formation as typically observed for other ultrasmall nanoparticles under such conditions.[67] In a final step, we develop an enterically-coated pill formulation for

C' dots, that in future studies could be employed to protect potentially sensitive ligands (*e.g.*, cytotoxic drugs) from degradation in the acidic stomach environment. The results described herein, in combination with encouraging earlier results of their behavior in several diagnostic and therapeutic human clinical trials upon local and intravenous injections, respectively,[25,68] suggest that ultrasmall, fluorescent, and PEGylated core-shell silica nanoparticles (C' dots) are a viable nanoparticle platform candidate for oral delivery in patients. This is a substantial finding as C' dots, in contrast to other experimental nanoparticle systems studied for oral delivery, have a proven pathway toward clinical translation. Furthermore, our results may generate renewed interest in examining the safety and health benefits of silica given its use across different stages of food production.

2. Results and Discussion

Fluorescent and PEGylated core-shell silica nanoparticles were synthesized via two main synthesis pathways as described in previous reports and illustrated in **Figure 2**a,b.[50,69] Smaller nanoparticles with hydrodynamic diameters of 5.0, 5.2, 6.3, 10.0, 18.9, and 24.7 nm, as determined by confocal FCS (Figure 2c and Figure S1, Supporting Information), were synthesized with the same method originally developed to produce ultrasmall C' dots (Figure 2a).[50] In short, tetramethoxysilane (TMOS) was co-condensed with an organic dye-silane conjugate (Cy5-silane or ATTO647N-silane) in an aqueous solution at a pH ≈8 to form fluorescent silica cores encapsulating covalently bound dye preventing dye leaching. For the smallest sets of nanoparticles (5.0, 5.2, and 6.3 nm), the growth was terminated by the addition of PEG-silane.[54] For nanoparticles 10.0, 18.9, and 24.7 nm in diameter, silica core size was further increased via silica shells added to the un-PEGylated particle cores by dosing tetraethoxysilane (TEOS) until the desired size was reached. In all cases, silica core synthesis was followed by PEGylation with an oligomeric PEG-silane containing 6–9 ethylene oxide units (PEG(6-9)). Both sets of particles were then heated at 80 °C for 24 h to finalize the PEGylation process.[50,54]

Larger PEGylated silica nanoparticles with hydrodynamic diameters above 25 nm (i.e., 26.0, 33.9, and 47.1 nm), were synthesized with a seeded growth method using L-arginine as the base catalyst (Figure 2b).[69] Briefly, TEOS was carefully added in four sequential steps to the surface of an aqueous solution containing L-arginine at 60 °C. Since TEOS does not mix with water, it forms a thin TEOS layer above the water solution, allowing interfacial hydrolysis of TEOS only, thereby controlling the rate of active silicic acid monomer formation entering the aqueous phase. Seed particle growth was further controlled by L-arginine, which both acts as a catalyst and associates with the silica particle surface, thereby further lowering the condensation rate onto the particle and increasing the degree of control over the process.[70,71] After TEOS-based seed formation, Cy5-silane was added dropwise to the seed solution followed by further TEOS addition to the aqueous solution surface in order to grow further silica shells similar to the first route (vide supra) and reach the desired particle diameter. Finally, PEG(6-9)-silane was again added before the solutions were heated at 80 °C for 12 h to promote covalent attachment of PEG-silane to the silica core (Figure 2b) and provide a similar size PEG shell to all particles of this study.

After synthesis, particles obtained from both formation pathways were purified via gel permeation chromatography (GPC) and thoroughly characterized with a combination of confocal FCS, UV–vis spectroscopy, and transmission electron microscopy (TEM) to obtain average hydrodynamic size (FCS), concentration and dyes per particle (FCS + UV–vis), and silica core size and size dispersity (TEM) (Figure 2c–g, Figure S1 and Table S1, Supporting Information), as extensively described in previous studies.[50,72,73] Confocal FCS autocorrelation functions (ACF) of these nanoparticles in deionized (DI) water appeared biphasic which can be attributed to either photo-induced *cis-trans* isomerization in Cy5 or to ATTO647N entering the triplet state.[73] These photophysical contributions can be quantitatively accounted for during fitting for all particles from individual synthesis batches (Figure S2, Supporting Information). As expected, with increasing particle size, FCS correlation curves (Figure 2c and Figure S1a, Supporting Information) shifted to longer time scales as larger particles diffused more slowly through the same focal volume of the objective in the confocal FCS setup. Larger particles also scatter light more strongly, which is manifested by the increasing scattering background with size in the optical absorbance spectra (Figure 2d). Finally, TEM demonstrated the near-spherical shape of the different particles as well as their reasonably low size dispersity (Figure 2e–g and Figure S1b–g, Supporting Information).

An important structural aspect of these nanoparticles is that they all have an oligomeric PEG(6-9) shell.[74,75] In addition to providing steric stability,[54] the neutral PEG surface layer allows for less hindered diffusion through mucus due to the lack of strong electrostatic interactions.[22,76,77] Past studies involving silica nanoparticles for oral applications were performed with non-PEGylated particles, which may contribute to the limited number of silica nanoparticles that have successfully been administered orally.[44,46,78]

Interactions with biological environments are sensitive to particle surface charge, so it was desirable to also characterize this property for our size series of silica nanoparticles. To that end, we performed zeta potential measurements on the different particles synthesized in this study. Results (averages of triplicate measurements) are summarized in Table S2, Supporting Information, with individual data sets shown in Figure S3, Supporting Information. Synthesis of particles with diameters of 10 nm or lower led to homogeneous zeta potential distributions and slightly negative zeta potentials between −5 and −10 mV, as expected from this optimized synthesis regime.[54] Generally, particles with sizes above 10 nm showed more heterogeneous distributions of zeta potentials, which was particularly true for the larger samples of 26.0, 33.9, and 47.1 nm synthesized via the L-arginine method. With the exception of particles with a diameter of 24.7 nm, the larger than 10 nm particles displayed slightly more negative average zeta potentials than the below 10 nm dots with values around −15 mV, suggesting that their PEG surface layer is not as dense as that of the smaller sets of particles,[54] thus exposing more of the anionic silica core surface.

To begin the investigation into the diffusion of sub-50 nm nanoparticles in mucus, we first prepared reconstituted porcine gastric mucin according to previously published protocols and compared our rheological results to those in the literature.[79,80] As the viscoelastic properties of mucus are strongly pH

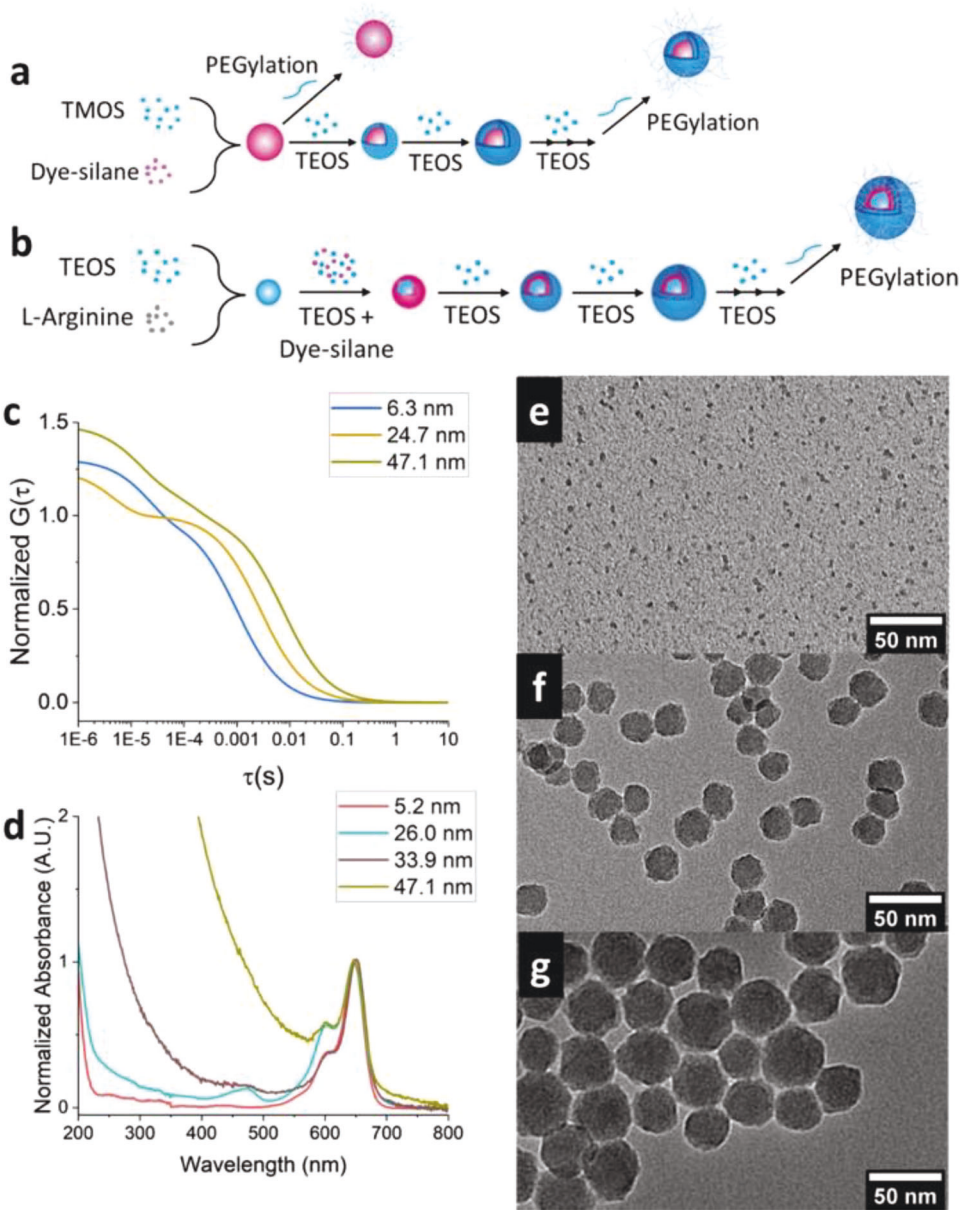

Figure 2. Synthesis workflows of the two routes used in this study to synthesize fluorescent core-shell silica nanoparticles of different sizes and characterization of select nanoparticles. a) Nanoparticles with hydrodynamic diameters below 25 nm were synthesized by co-condensing TMOS and dye-silane in an aqueous solution followed by PEGylation, with optional TEOS-based shell addition(s) until the desired size was reached, and terminated by PEGylation. b) Nanoparticles with hydrodynamic diameters above 25 nm were formed by adding TEOS and dye-silane-based shells to silica seeds grown in an L-arginine/DI water solution until the desired size was achieved and growth terminated by PEGylation. c) Representative normalized confocal FCS results for 6.3, 24.7, and 47.1 nm diameter nanoparticles (in DI water) with larger nanoparticles exhibiting longer diffusion correlation times than smaller ones. d) UV–vis absorbance spectra of 5.2, 26.0, 33.9, and 47.1 nm nanoparticles normalized to dye absorption peak. With increasing particle size, the increasing scattering background at shorter wavelengths can clearly be discerned. e–g) Representative TEM images of e) 6.3, f) 24.7, and g) 47.1 nm diameter nanoparticles, respectively. For complete data sets see Supporting Information.

dependent, we focused on mucus adjusted to a neutral pH of around 7.4 to coincide with the physiologically relevant pH found in the majority of the small intestine.[79,81] To ensure that the reconstituted mucus had similar properties to that of freshly harvested mucus, we performed rheological measurements on five independently reconstituted and pH-adjusted mucus samples and then compared results to existing literature data for freshly harvested mucus (Table S3, Supporting Information).[81–83] We observed reasonably good agreement between the two types of mucus and decided to continue with reconstituted porcine gastric mucins as our test mucus for diffusion studies. Previous studies of the diffusion of nanoparticles have used fresh, undiluted mucus collected from healthy human volunteers.[76] While ideal for testing, it is not always readily accessible. The low cost, rapid

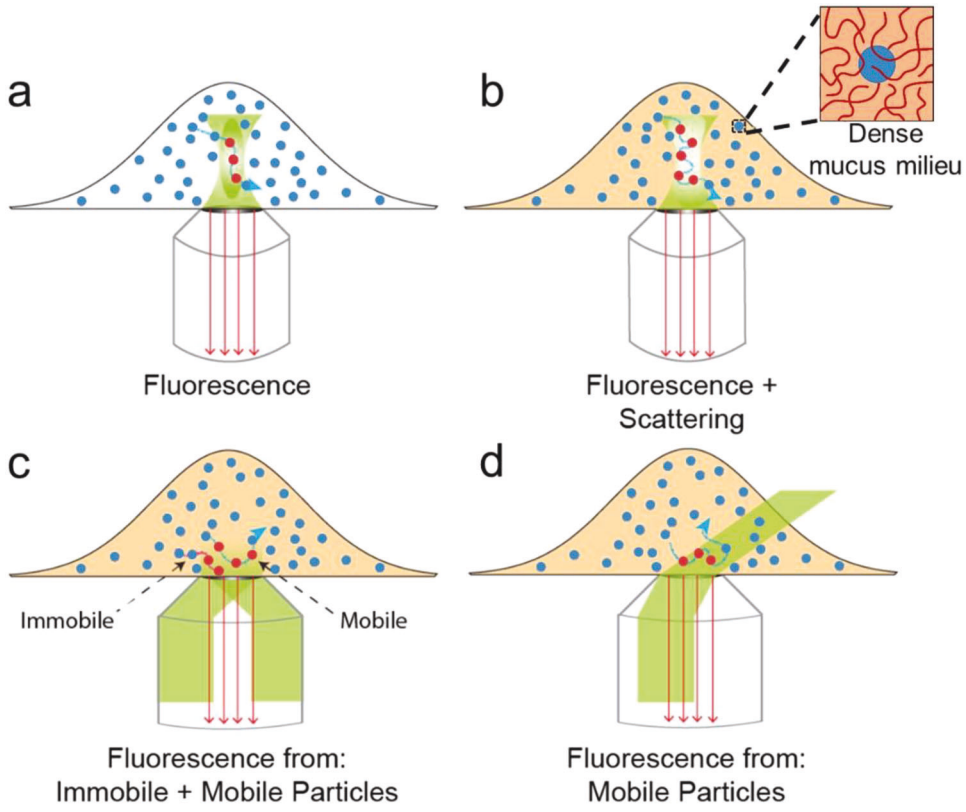

Figure 3. Nanoparticle diffusion in different media characterized via different FCS setups. a) Nanoparticles diffusing in DI water can conveniently be studied using confocal FCS. b) Confocal FCS cannot be used for analyzing nanoparticles diffusing in mucus due to the high scattering background of this medium. c) Imaging FCS using a TIRFM setup circumvents a high scattering background but is problematic when a subset of nanoparticles adheres to the glass substrate. d) Imaging FCS with a slightly non-critical angle of incidence (quasi) TIRFM setup enables the detection of signal primarily from particles diffusing above the glass substrate while simultaneously limiting the effects of scattering.

reconstitution, and near-unlimited supply of porcine gastric mucin make it attractive for initial nanoparticle screening before moving on to more complicated model systems.

When designing nanoparticles for oral delivery, their diffusivity in intestinal mucus is an important characteristic as faster diffusion has been shown to increase the probability of reaching the epithelial lining before the mucus is cleared and replaced in the GI tract.[84] Confocal FCS, as we demonstrated in Figure 2c, is traditionally used to measure the diffusion of fluorescent nanoparticles in DI water. In confocal FCS, temporal fluorescence fluctuations from an ellipsoidal observation volume (*xy*-dimension ≈250 nm and *z*-dimension ≈1.5 µm; **Figure 3**a) are used for autocorrelation analysis, yielding a temporal ACF. Fitting ACF with appropriate theoretical models provides diffusion coefficients of the sample (vide supra). Unfortunately, confocal FCS measurements of the nanoparticles in mucus are significantly more complex. With its dense and heterogeneous composition, mucus is a highly scattering environment that makes meaningful confocal FCS measurements nearly impossible due to the distortion of the ellipsoidal observation volume (i.e., both the *xy*- and *z*-dimensions of the volume become poorly defined) by the scattering medium and the high scattering background (Figure 3b).[85]

To analyze the diffusion of nanoparticles in mucus, instead, we employed imaging FCS which can simultaneously measure the average diffusion of an ensemble of particles in 25 independent 1.6 × 1.6 µm square spots.[66] Such high-throughput measurements greatly improve the statistics of diffusion data and thus the precision of diffusion property assessments. In the original proposal of this modality,[86] the authors used total internal reflection fluorescence microscopy (TIRFM) which allows illumination of a thin fluorescent sample plane (thickness along *z*-direction ≈100 nm) close to the coverslip by an evanescent field (Figure 3c). A temporal image stack of this sample plane is recorded by a fast electron-multiplying charge-coupled device (EMCCD) camera. An EMCCD is an array detector, that is, the camera chip is spatially segmented in the *xy*-plane into multiple tiny 2D imaging units (pixels). Each pixel contains temporal fluorescence fluctuation data from an individual small observation volume available for FCS analysis.[87] Fluorescence fluctuations from each pixel are then processed to generate corresponding ACFs. A 5 × 5 pixel area on the camera chip provides 25 pixels (25 independent observation volumes), thus generating 25 ACFs from a single recording of a temporal fluorescence movie across that area. The 25 ACFs are then fitted to determine the diffusion coefficients for each pixel.

During our initial imaging FCS measurements on silica nanoparticles in mucus we used the above-described TIRFM mode for excitation. A significant subset of the silica nanoparticles adhered to the surface of the silicate glass substrate used in our imaging dish, however. Fluorescence from these

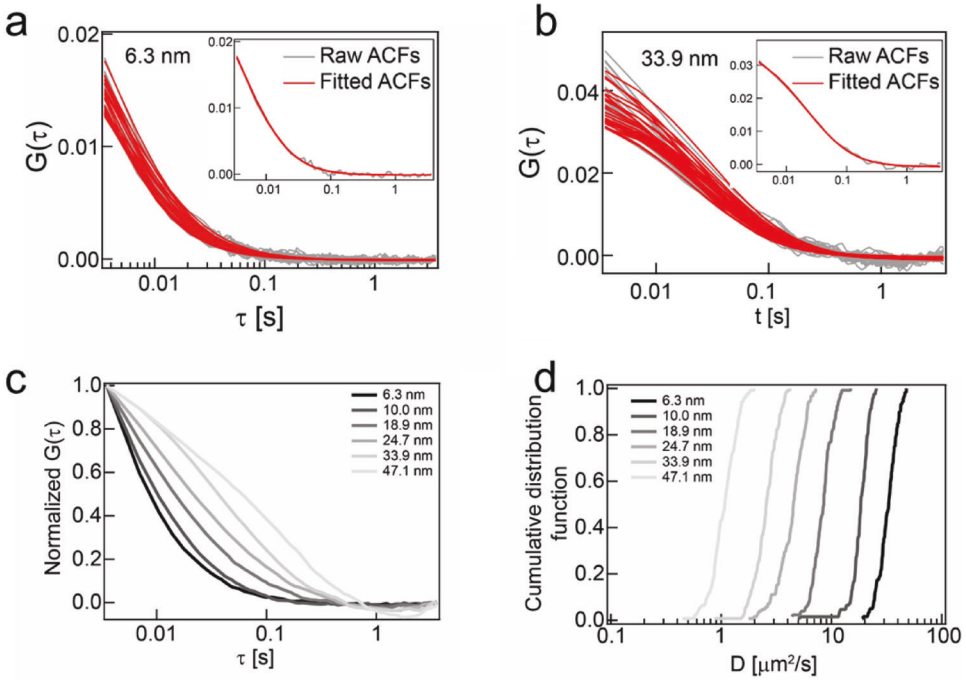

Figure 4. Results for nanoparticle diffusion in mucus obtained from quasi-TIRF-based imaging FCS. a) Ensembling of autocorrelation functions and fits of 6.3 nm particles diffusing in mucus. b) Ensembling of autocorrelation functions and fits of 33.9 nm particles diffusing in mucus. Insets in panels (a) and (b) show representative individual correlation curves of the ensembles with fits. c) Average autocorrelation functions (i.e., averages obtained from ensembles of ACFs obtained for each individual particle size, e.g., shown in panels [a,b]) for all nanoparticle sizes demonstrating the dependence of diffusion time on nanoparticle size. d) Cumulative distribution of D_{mucus} values demonstrating the change in diffusion coefficient in mucus as nanoparticle size changes.

immobilized particles increased the background under the fluorescence fluctuations of the diffusing particles, complicating imaging FCS analysis. Coating the surface of the imaging dish with a dense PEG layer (see Supporting Information) to suppress particle adhesion did not completely eliminate the issue. Instead, we modified the illumination scheme by using a quasi-TIRF or leaky TIRF mode, which was originally employed to image a sample plane rising slightly above the glass surface using a TIRF microscope (Figure 3d).[88–91] This scheme was later used in EMCCD-based FCS for diffusion measurements in solution.[92] Here, the incident angle of the excitation laser beam is kept at a value slightly smaller than the critical angle of the oil/water interface. Since the incident angle criteria is not fulfilled, TIR does not occur in this scheme and thus the thin sample plane parallel to the PEGylated glass substrate is not illuminated. Rather, the excitation beam passes through an inclined sample plane slightly away from the PEGylated glass substrate. At the same time, the axial depth of this scheme is still limited, thus decreasing the impact of the high scattering background of the mucus samples.

In this manner, the nanoparticles immobilized on the glass surface remain dark (not excited due to the absence of an evanescent field) while the mobile nanoparticles in the mucus sample in the inclined sample plane are illuminated. Temporal fluorescence fluctuations from this plane arising from particles diffusing through this plane are recorded by the EMCCD camera. Raw ACFs from multiple adjacent pixels can then be fitted to simultaneously yield a diffusion coefficient for each pixel.

With this quasi-TIRFM setup, we recorded a stack of 20 000 frames with an integration time of 3.5 ms for reconstituted mucus samples separately containing the differently sized nanoparticles (i.e., 6.3, 10.0, 18.9, 24.7, 33.9, and 47.1 nm). Since the major contribution to fluorescence fluctuations in this setup comes from particle diffusion, performing autocorrelations of the fluorescence fluctuations of the entire stack as a function of time allowed calculation of the particle diffusion coefficient in mucus (D_{mucus}) by fitting to the diffusion model as described in the Supporting Information (Equation (S8), Supporting Information). As is apparent from comparison of results for two specific particle sizes of 6.3 and 33.9 nm (**Figure 4**a,b) as well as from the average ACFs for all nanoparticle sizes measured (Figure 4c), there was a clear increase in lag time, τ, associated with increasing particle diameter: Larger particles diffused slower in mucus than smaller ones, as expected. As the cumulative distribution functions of the calculated values of D_{mucus} from individual measurements for the differently sized nanoparticle batches demonstrate (Figure 4d), the average values of D_{mucus} for the different nanoparticle sizes were distinctive and quantifiable.

For comparison, diffusion coefficients in DI water, D_{water}, were obtained from fits of confocal FCS-derived ACFs (Equation (S3), Supporting Information) for all tested nanoparticles shown in Figure 2c and Figure S1a, Supporting Information. When plotting D_{water} and D_{mucus}, respectively, versus 1/diameter (**Figure 5**a,b) as determined by TEM (Table S1, Supporting Information), both decreased monotonically with size. Furthermore, due to the higher viscosity of mucus compared to that of DI

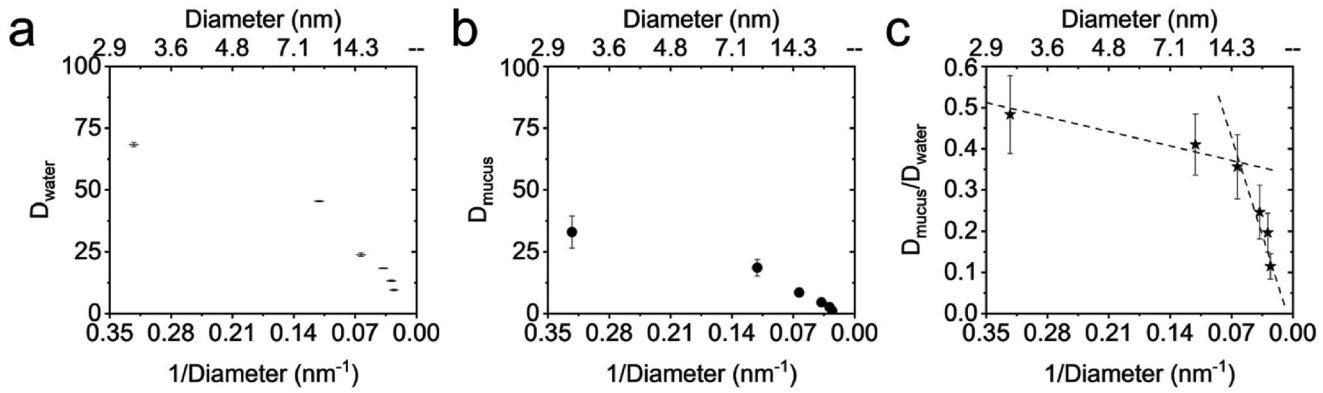

Figure 5. Comparison of nanoparticle diffusion in DI water versus mucus. Error bars (SD) for D_{water} resulted from averaging three confocal FCS measurements per nanoparticle size; errors (SD) for D_{mucus} resulted from averaging over ensemble measurements of the imaging FCS. Nanoparticle size was determined based on TEM. The diffusion coefficients of nanoparticles decrease monotonically as size increases in both a) DI water (D_{water}) and b) mucus (D_{mucus}). c) Taking the ratio of D_{mucus}/D_{water} demonstrates that nanoparticles diffuse slower in mucus than in DI water and that particles < 20 nm diameter appear to follow a different trend than those > 20 nm. Propagation of error was used to compute the error bars in panel (c).

water, $D_{mucus} < D_{water}$ for all particle sizes measured, as expected (compare Figure 5a,b). When we took the ratio of D_{mucus}/D_{water} (Figure 5c), which signifies how fast a nanoparticle diffuses in mucus relative to DI water, we observed two distinct regimes of particle behavior with two different apparent slopes merging at a critical nanoparticle diameter of ≈20 nm. Nanoparticles with diameters < 20 nm exhibited significantly improved diffusion characteristics when compared to nanoparticles with larger sizes that were substantially more hindered in their mucus diffusion. Most importantly, when compared to the literature,[93] the values of D_{mucus} ranging from ≈1–33 μm^2 s^{-1} and associated ratios, D_{mucus}/D_{water}, ranging from ≈0.1–0.5 for all nanoparticle sizes tested are sufficient for fast enough diffusion through the mucus layer to reach the epithelial layer before the mucus would be replaced. For humans, this translates to a particle crossing 100 μm of mucus (the thickness of the mucus layer in the intestine) in less than 240 min.[93] Based on measured values of D_{mucus}, the 6.3 nm particles would traverse that distance in just 11 s, while the 47.1 nm particles would still only take 5.5 min to cross the mucus layer, far faster than the required 240 min.[93]

The favorable outcomes of particle mobility in mucus, especially for ultrasmall particle sizes, encouraged us to investigate the second major barrier for oral delivery associated with the epithelial lining. The standard assay used to study the permeability of compounds through a Caco-2 cell monolayer involves growing the cells in a Transwell dish on a semipermeable membrane (**Figure 6**a). After the cells have formed a monolayer, the compound of interest is added to the apical side (on top of the cells) at a known concentration and allowed to incubate with the cells for a specified amount of time. Following incubation, the concentration of the compound of interest on the basolateral side (below the cells and semipermeable membrane) is measured. Equation (1) is used to determine the apparent permeability (P_{app}) of that compound across the Caco-2 monolayer, where dQ/dt is the molar flux into the basolateral side, A is the surface area of the semi-permeable membrane, and C_0 is the initial concentration on the apical side.[39] As mentioned earlier, higher values of P_{app} have been shown to correlate with greater oral bioavailability in human patients, with compounds exhibiting $P_{app} > 1 \times 10^{-6}$ cm s^{-1} demonstrating almost complete uptake.[35,36,39]

$$P_{app} = \frac{dQ}{dt} \times \frac{1}{A \times C_0} \quad (1)$$

To ensure that the monolayer well resembled the epithelial lining of the GI tract and formed tight junctions, we used Lucifer yellow (LY) as a standard. It has been reported that the integrity of a Caco-2 monolayer is good if the P_{app} of LY across the monolayer is below 5×10^{-7} cm s^{-1}.[94] The measured values of P_{app} of LY across all Caco-2 monolayers (see Supporting Information for more details) used in this study are depicted in Figure 6b (blue and red data sets represent the results of two independent cell passages). All P_{app} values were $< 3 \times 10^{-7}$ cm s^{-1}, signifying that these monolayers passed this quality test and were ready for nanoparticle experiments.

We next examined the apparent permeability of PEGylated fluorescent core-shell nanoparticles with 6.3, 24.7, and 33.9 nm hydrodynamic diameters used in the diffusion studies, that is, sizes that are below, similar to, or significantly above the critical size threshold of ≈20 nm observed in the mucus diffusion experiments. These were tested on the same exact group of Caco-2 cells subjected to the Lucifer yellow assay. The resulting values for the P_{app} of nanoparticles across the Caco-2 cell monolayer are shown in Figure 6c (depicted in blue). The side-by-side comparison between P_{app} values of LY and those of the nanoparticles through the same membrane (compare Figure 6b,c) demonstrates that permeabilities of LY were comparable to those of much larger ≈25 nm sized particles and substantially lower than those of the smaller ≈6 nm particles, despite the latter being substantially larger than this dye molecule with hydrodynamic size of only 1–2 nm. These results clearly suggest that size is not the only parameter that governs permeability through such cellular membranes. Comparing P_{app} between different particles in Figure 6c showed that beyond the 6 nm-sized particle, permeability significantly decreased as particle size increased, with the value for the largest 33.9 nm particles being essentially undetectable due to the vanishing permeability at that size. This study

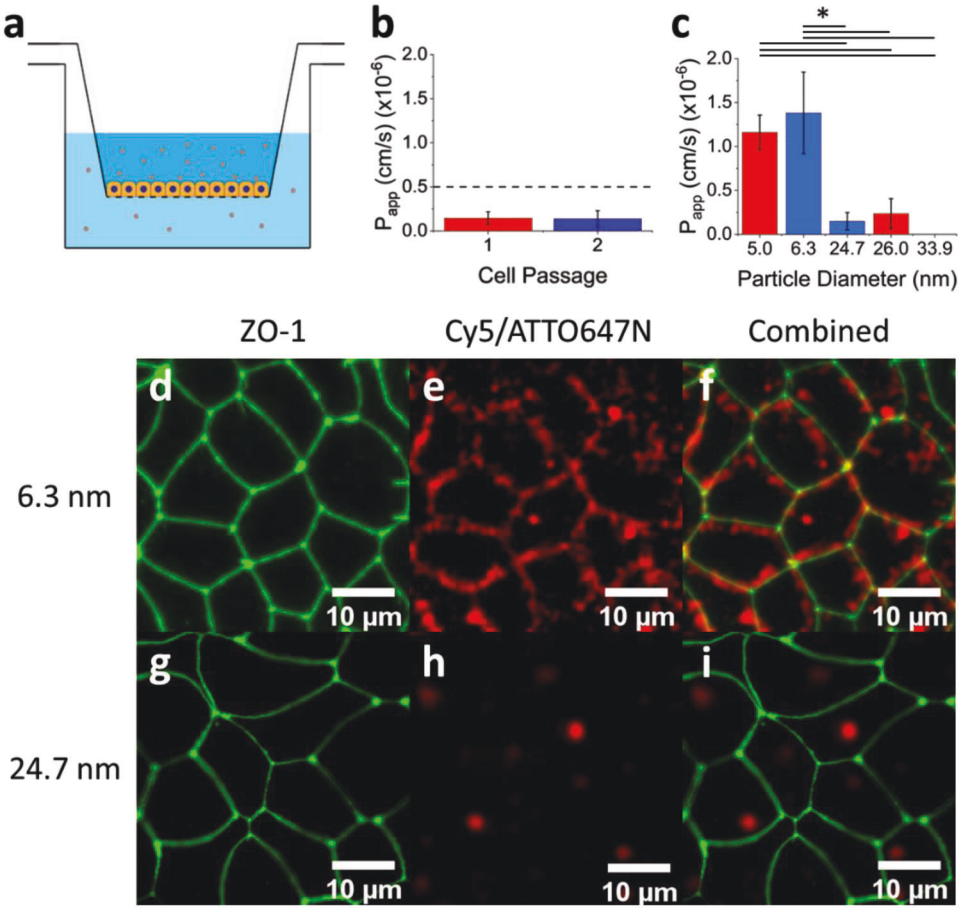

Figure 6. Caco-2 permeability assay results for nanoparticles of different sizes. a) Schematic of the Transwell assay used to study the permeability of nanoparticles through the Caco-2 monolayer. b) Results from the LY assay demonstrating that all Caco-2 cell monolayers used from two different cell passages had well-formed tight junctions. Passage 1 (red) was used for the 5.0 and 26.0 nm nanoparticles, while passage 2 (blue) was used for the 6.3, 24.7, and 33.9 nm nanoparticles shown in panel (c), respectively. c) Apparent permeability (P_{app}) of nanoparticles through the Caco-2 monolayers, which decreased as nanoparticle size increased, with the 33.9 nm nanoparticle permeability being undetected. Measurements from three separate Caco-2 wells per cell group were averaged to generate values of P_{app} and associated error bars (standard deviation) in (b,c). d–i) Fluorescence laser scanning confocal microscopy of fixed Caco-2 cells using d,g) green and e,h) red channels to visualize junctions and particles, respectively. Membranes were exposed to either d–f) 6.3 or g–i) 24.7 nm silica nanoparticles (Cy5 or ATTO647N, red). Tight junction protein ZO-1 (green) was immunostained using Alexa Fluor 488-antibody conjugates (green). * $p < 0.0001$ as determined via ANOVA and Tukey's post-hoc analysis with $n = 3$.

was subsequently replicated with nanoparticles of similar sizes (i.e., with 5.0 and 26.0 nm particles) on an entirely separate Caco-2 cell passage, yielding similar results (Figure 6c, depicted in red). It is worth noting that despite differences in their synthesis (Figure 2a,b) and resulting zeta potential (−7.0 vs −16.2 mV), the permeabilities of the 24.7 and 26.0 nm particles were very similar, suggesting that surface charge differences displayed by the different particle batches did not contribute substantially to the permeability results. Interestingly, when moving from 6.3 to 5.0 nm particles, permeability did not continue to increase, counter to expectations, perhaps indicating that permeability is not very sensitive to size in this ultrasmall particle size regime. This observation is consistent with the smallest object tested, that is, organic reference dye LY, displaying a substantially lower permeability than the smallest particles despite their substantially larger size (vide supra). Finally, the values for $P_{app} > 1 \times 10^{-6}$ cm s^{-1} measured for the two ultrasmall nanoparticles (i.e., for 5.0 and 6.3 nm silica nanoparticles referred to as C' dots) suggest that they may be suitable for oral delivery applications in humans.[35,39]

A separate study, while not using particles in the ultrasmall size regime, investigated the role of size, shape, and surface chemistry on permeability.[40] Values of P_{app} observed for our ultrasmall C' dots are similar to those of other ultrasmall nanoparticles, albeit with different compositions.[95] The finding that silica nanoparticles, particularly the ultrasmall particles with diameters < 10 nm (the C' dots), could permeate Caco-2 monolayers with permeabilities above 1×10^{-6} cm s^{-1} is significant, as no other silica nanoparticle, to the best of our knowledge, has demonstrated permeation across these cell layers without being surface functionalized with compounds detrimental to their overall biocompatibility.[44,46–48] Furthermore, to the best of our knowledge, no other organic-inorganic hybrid nanoparticle platform with IND FDA approval for human clinical (diagnostic and therapeutic) trials – providing a proven pathway towards clinical translation – has exhibited such high Caco-2 monolayer

permeabilities. As mentioned earlier, silica nanoparticles that have been studied to date were all above 20 nm in diameter and were not PEGylated, both likely contributing factors to their inability to traverse these Caco-2 cell monolayers. Finally, it was observed that nanoparticles with a diameter well above 25 nm had a P_{app} below the detection limit of this cell system, consistent with literature findings.

To better understand the mechanism by which these core-shell silica nanoparticles traverse the Caco-2 cell monolayer, we repeated the Caco-2 permeability experiments using the 6.3 and 24.7 nm particles, fixed the cells, immunostained the ZO-1 tight junction protein, and performed fluorescence laser scanning confocal microscopy to localize these particles in relation to the tight junctions (see Supporting Information for details).[44] From the results shown in Figure 6d–f, the ultrasmall (6.3 nm) C' dots (red) preferentially localized near tight junctions (green). Images also exhibited sparsely distributed puncta that likely stemmed from endosomal uptake of the particles.[96,97] In surprisingly sharp contrast, only intracellular puncta were visible in the cells exposed to the 24.7 nm nanoparticles (Figure 6g–i). Experiments were repeated on a separate Caco-2 cell passage leading to similar observations corroborating the results (Figure S4, Supporting Information). Collectively, these data suggest that the higher permeability of ultrasmall C' dots across the Caco-2 membrane is likely attributable to substantially enhanced passive (i.e., through cell-cell junctions) transport relative to active (i.e., through the cells) transport, while the 24.7 nm nanoparticles preferentially participate in an active transport mechanism.

The favorable outcomes of ultrasmall particle mobility in mucus and permeability through a Caco-2 cell monolayer encouraged us to further expand the assessment of their behavior in the context of oral delivery. Prior to reaching the small intestine, orally administered nanoparticles would have to traverse the acidic environment of the stomach. For cases not using a pill formulation with protection via a specific coating against the low stomach pH (vide supra), it is of interest to study the ability of ultrasmall and PEGylated fluorescent core-shell silica nanoparticles (C' dots) to survive conditions found in the stomach. To that end, we investigated their stability in three different environments: artificial gastric juice, pH 1.5 HCl, and pH 13 NH_3. Artificial gastric juice (pH 1.5) is an aqueous solution mainly comprising HCl, NaCl, and pepsin that simulates the contents of the stomach. For comparison, pH 1.5 HCl was used to demonstrate purely acidic pH effects on particle stability, while pH 13 NH_3 was employed as a positive control as such strongly basic pH conditions are known to dissolve silica.[98] 100 µL of 120 µM Cy5-C' dots were diluted into 300 µL of either gastric juice, HCl, or NH_3 solutions and placed on a tube rotator at 37 °C. Small aliquots were taken every 15 min over a 2-h period, on which confocal FCS was performed to track particle size over time. These conditions were chosen by taking into account the maximum volume of gastric acid in a mouse stomach, the total internal volume of a mouse stomach, and the expected residence time of ≈1 h within the stomach.[99–101] From results displayed in **Figure 7**a, ultrasmall C' dots exhibited no significant size change over the 2-h period in both the gastric juice and pH 1.5 HCl, while their diameter monotonically decreased within that time frame when exposed to pH 13 NH_3. Silica has previously been shown to be metastable at pH < 4, but to dissolve at pH > 11, so these findings are consistent with earlier literature reports.[102] These data suggest that C' dots in their standard formulation, without any further protection, are already able to survive the stomach's acidic environment and therefore should be suitable for oral administration.

The limitations of predicting human outcomes on oral bioavailability from animal studies are well documented.[103,104] As a result of the experiments described in earlier sections, we still thought it instructive to perform oral delivery screening experiments with ultrasmall and PEGylated fluorescent core-shell silica nanoparticles (C' dots) in a small number of mice to achieve a qualitative assessment of their potential in vivo. To that end, eight B6 (C57BL/6J) mice were used in this study, with five mice each being administered 100 µL of 120 µM 5.2 nm Cy5-C' dots via oral gavage, and three control mice each being administered 100 µL of saline. Earlier quantitative BD and PK studies using positron emission tomography (PET) after intravenous injection of radioisotope labeled samples in animal models and human patients established that ultrasmall C' dots are efficiently cleared through the renal system once they are in the bloodstream due to their ultrasmall size.[24–26,61] Therefore, analysis of animal urine after oral gavage appeared to be an appropriate reliable, quick, and qualitative screening method to determine if any particles were successfully taken up through the small intestine into the bloodstream and subsequently renally cleared. To maximize the volume of urine collected for analysis, all mice were housed in individual metabolic cages. Urine collected prior to dosing was considered the 0 h time point. Pooled urine samples collected immediately after dosing up to 12 h as well as between 12 and 24 h post-administration were considered the 12 and 24 h time points, respectively. From the comparison of fluorescence spectra in Figure 7b, urine at the 24 h time point of mouse 2 and mouse 3 after oral gavage of C' dots exhibited a signal well above that of urine from a saline control mouse. Furthermore, the shape of the fluorescence signal was consistent with that of a reference sample of Cy5-C' dots in DI water. Urine samples of all animals administered C' dots, either at the 12 or 24 h time points or both, exhibited higher fluorescence intensities as compared to saline control urine and showed fluorescence intensity distributions consistent with Cy5-dye fluorescence (Figure S5, Supporting Information). These results suggested the presence of fluorescent Cy5-C' dots in the urine of all five mice tested after oral gavage.

To corroborate the presence of ultrasmall and PEGylated fluorescent core-shell silica nanoparticles (C' dots) in urine after oral gavage, we used confocal FCS as a second method for particle detection. FCS is a very sensitive technique (down to nM concentrations) and provides size information of the diffusing fluorescent objects, here in urine.[73,105] In Figure 7c, as a control, the ACF of Cy5-C' dots added to urine obtained from mice before oral gavage ("Reference C' dots in urine") was compared to the same urine without C' dot addition ("0 h urine") as well as to a saline control sample 24 h after oral gavage ("24 h Saline Control"). This comparison illustrated that in these measurements the unambiguous detection of C' dots was straightforward as ACFs of urine samples containing C' dots were very different from those without (i.e., plain urine). Indeed, the FCS ACFs of the two C' dot-containing urine samples identified in Figure 7b exhibited diffusion characteristics expected for C' dots in solution (Figure 7d). Interestingly, however, the two curves are not exactly on top of each other. Data of the urine sample from mouse 2 reflects slightly slower

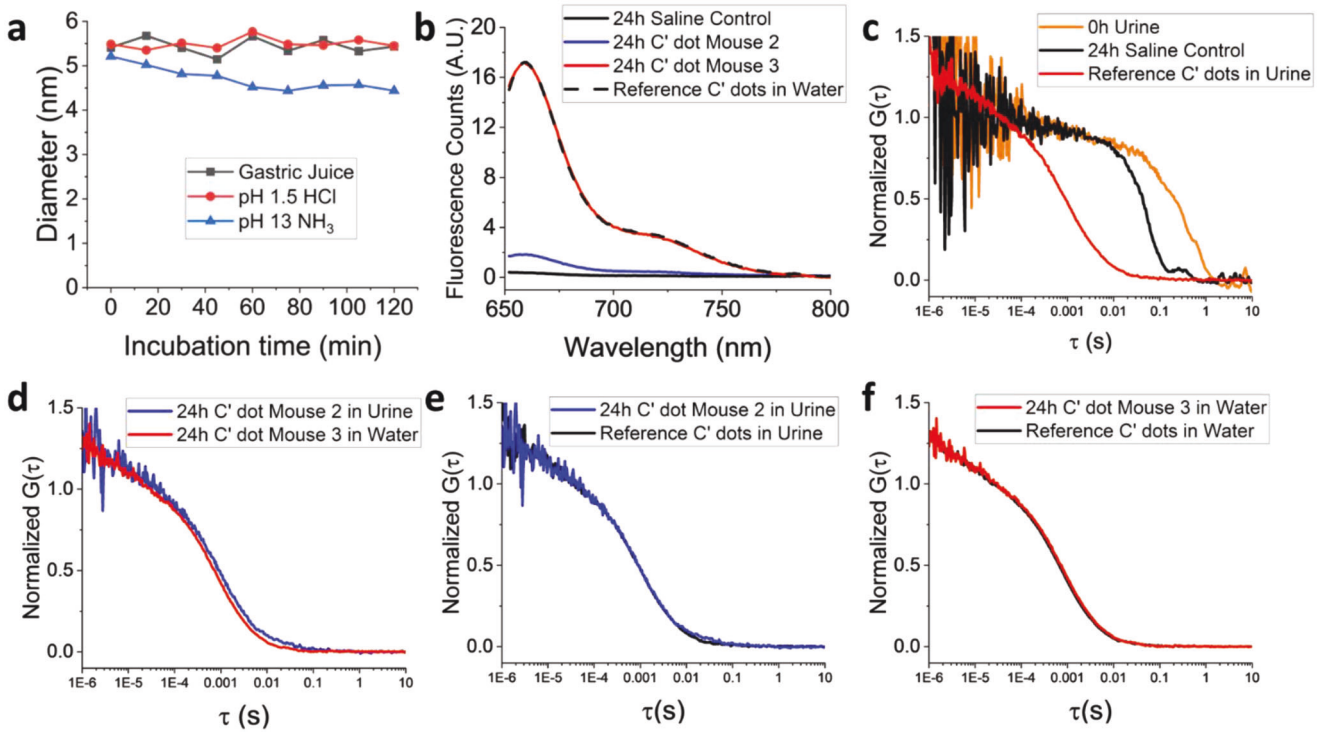

Figure 7. Nanoparticle stability in artificial gastric juice and fluorescence analysis of urine from mice administered 5.2 nm silica nanoparticles (C' dots) orally. a) FCS-derived particle size versus time of C' dots incubated in either artificial gastric juice, pH 1.5 HCl, or pH 13 NH_3. b) Fluorescence (emission) spectra of urine collected from three separate mice 24 h after either oral administration of either C' dots (mouse 2 and mouse 3) or saline control compared to a Cy5-C' dot spectrum (dashed line) in DI water normalized to the mouse 3 urine. c) FCS curves of urine collected from two mice without C' dot administration (either immediately prior to C' dot administration [0 h] or 24 h after administration of saline) compared to C' dots diluted in mouse urine collected separately. d) FCS curves of urine collected from two separate mice 24 h after administration of C' dots, with one sample (red curve) being diluted in DI water due to its high initial concentration, revealing differences in autocorrelation times. e,f) Comparison of FCS curves of samples in panel (d) with associated references: The undiluted urine sample in panel (d) is compared to a mixture of the same C' dots added to mouse urine, while the diluted urine sample is compared to the same C' dots in DI water. Results suggest that differences in panel (d) are likely attributed to viscosity differences between urine and DI water.

particle diffusive motion than that of mouse 3 (typically indicative of larger object size), which was diluted with DI water due to its higher initial concentration (Figure 7d). To identify the origin of this deviation, we showed that these results can be respectively reproduced by adding 5.2 nm Cy5-C' dots directly to either plain urine or DI water (Figure 7e,f). This suggests that the slower diffusion of particles in mouse 2 urine is not actually caused by a larger particle size but instead is caused by the higher viscosity of urine compared to DI water. Using the Stokes–Einstein equation (Equation (S4), Supporting Information,), we estimated that the viscosity of urine is ≈1.2 times higher than that of DI water, consistent with values reported in the literature.[106,107] FCS data sets for all urine samples from the eight mice studied at different time points after oral gavage of saline or C' dots are shown in Figures S6 and S7, Supporting Information, respectively. Overall, all five mice administered particles showed FCS ACFs consistent with C' dots present in their urine at the 12 h time point, with three of these mice additionally showing such ACFs at the 24 h time point.

Taken together, these data demonstrate that orally administered ultrasmall and PEGylated fluorescent core-shell silica nanoparticles referred to as C' dots successfully travel through the stomach, intestinal mucus, intestinal epithelia, and into the bloodstream of mice from where they are renally cleared. It is noteworthy that the size of C' dots after oral gavage and passage through these complex biological environments remains unchanged, that is, their size exactly matches that of pristine parent C' dots (see Figure 7e,f). This suggests that the particles are neither degraded, for example, through passage through the acidic stomach environment, nor suffering from the build-up of a protein corona, for example, from circulation in the bloodstream, often encountered for other (ultrasmall) particle platforms.[67] In regards to the latter, the covalent bonding of the PEG-silane ligands to the silica core surface via up to three covalent Si-O-Si bonds per PEG-silane leads to a dense and robust PEG brush that makes ligand exchange reactions, for example, expected in blood serum for non-covalent thiol- (or amine-) linkages to ultrasmall metal nanoparticle cores, unlikely.[54] Finally, observing 5.2 nm C' dots in the urine of all mice after oral gavage further adds to the positive outcomes of the studies reported here concerning the potential of ultrasmall C' dots for oral administration. Together with earlier reports on their safe use in human clinical trials,[25,68] these studies suggest that C' dots are viable candidates for further oral delivery studies. Such studies could entail, for example, the use of radioisotope-labeled particles enabling quantitative positron emission tomography (PET) investigations. In

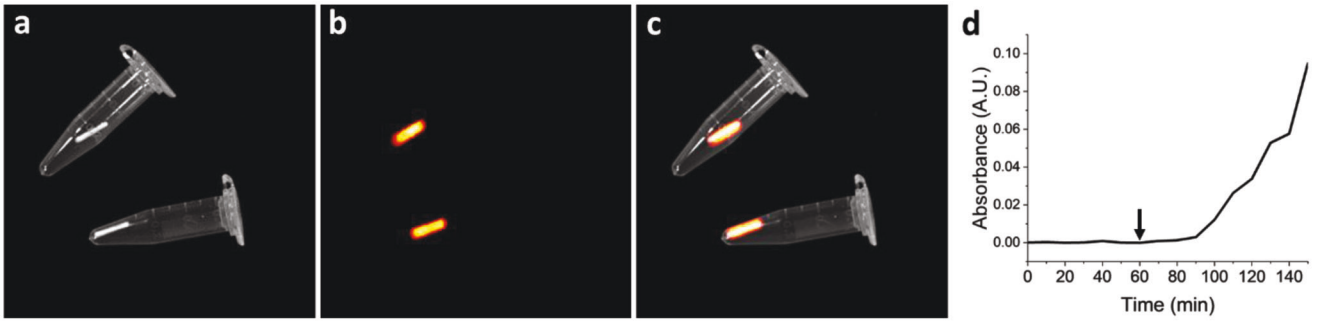

Figure 8. Nanoparticle pill formulation and pill dissolution study. a) Photo of a C' dot pill formulation inside two 1.5 mL microcentrifuge tubes. b) Fluorescence image of pill formulation in (a) using an IVIS imaging system with a 660 nm emission filter. c) Overlay of pill photo and pill fluorescence image. d) Dissolution of pill when transferred from artificial gastric juice to pH 7.4 PBS (at time point denoted by arrow) as evidenced by measuring Cy5-C' dot absorption over time.

contrast to the qualitative assessments based on optical signals and incomplete urine collection described here, which preclude assessment, for example, of the exact fraction of particles renally cleared, such PET-based analyses would provide quantitative descriptions of particle biodistribution (BD) and pharmacokinetics (PK) necessary to fully assess their potential for oral delivery.[25]

As a final step towards the translation of ultrasmall and PEGylated fluorescent core-shell silica nanoparticles (C' dots) to a formulation suitable for oral administration, we generated a procedure to encapsulate C' dots in a pill (**Figure 8**). This is particularly important for scenarios when C' dots are carrying sensitive payloads (e.g., cytotoxic drugs) that may be degraded by the acidic environment of the stomach. In short, maltodextrin was used as a matrix agent and added to the receiving chamber of a gelatin pill (see Supporting Information). Ultrasmall C' dots suspended in 70% ethanol were then added, and the mixture was allowed to form a water-soluble gel. The pill was then closed, and food-grade shellac was used to coat the final, nanoparticle-loaded pill. The food-grade shellac acts as an enteric coating that protects the pill formulation from the low pH environment of the stomach. We showed that this nanoparticle pill formulation does in fact encapsulate C' dots which remain fluorescent as shown by obtaining fluorescence images in an IVIS imaging system equipped with a 660 nm emission filter (Figure 8a–c). We further showed that while this nanoparticle pill formulation exhibits negligible particle release in artificial gastric juice over a period of 2 h tested, it does significantly release C' dots at a pH similar to that found in the small intestine (Figure 8d). This was accomplished by placing pills into artificial gastric juice for 1 h and then transferring them to phosphate-buffered saline (PBS) with pH ≈7.4 for another 1.5 h. During this entire period, a small aliquot of solution was collected every 10 min for which the Cy5 absorbance was measured with a UV–vis spectrometer. In all, these results suggest that the pill formulation and coating could be suitable for protecting C' dots in the stomach while also acting as capable vehicles for oral particle delivery.

The observation of the successful passage of ultrasmall and PEGylated fluorescent silica nanoparticles through the stomach, intestinal mucus, intestinal epithelia, and into the bloodstream raises several interesting questions and provides opportunities for future investigations. It has been demonstrated that synthetic silica formation in water, employing hydrolysis and condensation reactions, for example, associated with alkoxysilanes or other silica precursors, proceeds via primary amorphous silica clusters of around 2 nm in size.[108] In biogenic silica formation, for example, associated with silica shells of diatoms (or radiolaria), similarly sized clusters of highly branched polysilicic acids with specific proteins (e.g., silaffins) are also present.[109] It is not difficult to imagine, therefore, that in the presence of natural macromolecules like polysaccharides or proteins capable of multidentate hydrogen bonding to surface silanol groups, ultrasmall hybrid core-shell silica nanoparticle architectures emerge with structural characteristics similar to those of the herein-discussed synthetic ultrasmall and PEGylated (fluorescent) core-shell silica nanoparticles. Furthermore, such biogenic ultrasmall particles present in natural food products, particularly in those considered "healthy food" (salads, grasses, seaweed, etc.), may display similar oral delivery properties as those discussed in this study. This sheds new light on questions about the BD, PK, function, and potential health implications associated with such ultrasmall silica nanomaterials. There are a few published reviews and studies discussing the potential health benefits of silica, for example, bone health, immune function, Alzheimer's disease, and atherosclerosis.[110–112] Postulated mechanisms include antioxidant effects and local effects, for example, on the gut-associated lymphoid system or the gut microbiota, though these are not completely understood.[113] Similar to the use of silica nanoparticles in therapeutic applications, their use in different stages of food production, including processing and packaging, is also increasing.[114] This will substantially increase oral exposure. If such silica is making its way to the bloodstream as we have demonstrated, both its safety and local effects need to be reevaluated. Some of the hypothesized mechanisms of action such as modulation of immune function and changes in gut microbiome may also be associated with anticarcinogenic effects of ultrasmall silica nanoparticles, including ferroptosis (involved in cancer immunotherapies like immune checkpoint blockade; ICB) and upregulation of the inflammatory cytokine genome and adaptive immune pathways, collectively referred to as "self-therapeutic" (C' dot) properties (vide supra).[51,63–65] Such initially surprising behavior may be rationalized considering that the most abundant oxide in the crust of planet Earth is silica and that living organisms have therefore evolved over millions of years

with various silica particulate structures, for example, in their environment, plants, and plant-based foods. Based on this perspective, the results of the study described herein certainly warrant further close examinations, for example, of the fascinating connection between ultrasmall silica in nutritional and therapeutic products and their safety and health benefits via both in vitro and in vivo works.

3. Conclusions

In conclusion, in this study we investigated the ability of fluorescent PEGylated core-shell silica nanoparticles with sizes systematically varied from ≈5 to 50 nm, that is, including, but not limited to, ultrasmall particles with sizes below 10 nm that are referred to as C' dots, to overcome the barriers associated with stomach acid, mucus, and epithelial lining, thereby assessing their potential for oral delivery. We demonstrated that from all sizes tested, particles with diameters below the cut-off for renal clearance (i.e., C' dots) exhibit properties that appear the most conducive to oral administration. In detail, by developing a reproducible method of mucus reconstitution from porcine gastric mucin and taking advantage of recent progress with an imaging FCS technique in combination with a quasi-TIRF microscopy setup, we first experimentally determined the diffusion coefficients, D_{mucus}, of PEGylated fluorescent core-shell silica nanoparticles with sizes ranging from ≈5–50 nm suspended in highly scattering mucus. When plotting the ratio of D_{mucus}/D_{water}, which represents the rate at which a nanoparticle diffuses in mucus relative to DI water, as a function of 1/diameter we observed two distinct regimes of particle behavior with two different apparent slopes intersecting at a critical nanoparticle diameter of around 20 nm. Above this size, particle diffusion was most progressively slowed by the local mucus environment. Subsequently, using the classic Caco-2 cell monolayer permeability assay, we observed that PEGylated fluorescent core-shell silica nanoparticles of the smallest sizes tested (i.e., C' dots) were able to permeate the cell monolayer most efficiently. Similar to the diffusion studies, a critical particle size of roughly 10–20 nm was identified where the mechanisms inducing permeability changed substantially. Larger particles (beyond around 30 nm) showed negligible permeability. Particles around 20 nm in size showed similar permeability to substantially smaller reference dye LY, while fluorescence microscopy was consistent with only an active transport mechanism of such particles through the cells. Ultrasmall particles with sizes below the cutoff for renal clearance (diameters < 10 nm, i.e., C' dots) showed the most promise by displaying permeabilities substantially higher than that of smaller reference dye LY, that is, above the critical value of 1×10^{-6} cm s^{-1}, correlated with full (i.e., 100%) absorption in humans.[35,39] For such small particles, in sharp contrast to particles around 20 nm in diameter, fluorescence microscopy results revealed a superposition of two mechanisms enabling cell membrane permeation. One mechanism was similar to that observed for larger particles showing sparsely distributed intracellular puncta consistent with active transport (through cells), while a second was characterized by high levels of colocalization with tight junctions consistent with passive transport mechanisms (through tight junctions). The result that densely PEGylated core-shell silica nanoparticles, particularly ultrasmall C' dots with diameters below 10 nm, can permeate the Caco-2 cell monolayer with permeabilities above 1×10^{-6} cm s^{-1} is significant as this has been one of the greatest factors limiting the oral administration of silica nanoparticles to date. The finding that ultrasmall C' dots exhibit high stability in gastric juice further suggests that their standard formulation may already be suitable for oral administration. A pill formulation was developed, nonetheless, in order to protect pH-sensitive payloads that may be attached, for example, to the C' dot silica surface via click chemistry.[57] Particle suitability for oral administration was further investigated by qualitative in vivo mouse screening studies suggesting orally administered C' dots were successfully taken up through the GI tract into circulation followed by renal clearance, the latter as unambiguously evidenced by a combination of fluorescence spectroscopy and FCS of urine samples. Importantly, these cleared particles retained the exact initial size and fluorescence characteristics as the particles before oral gavage, suggesting that no degradation in the stomach occurred and no protein corona was formed throughout their passage across different biological barriers. The lack of protein corona formation sets C' dots apart from other ultrasmall particle platforms.[67]

As discussed earlier, it is well-known that oral uptake studies in animal models are not predictive of uptake in humans.[103,104] However, our findings indicate that further studies into oral delivery of C' dots are warranted as they are, at the minimum, viable candidates for oral administration of either a "self-therapeutic" or cytotoxic drug-carrying particle to patients with a proven pathway towards clinical translation. This is informed by previous studies demonstrating, for example, favorable BD and PK profiles of targeted C' dots for safe use in humans,[25,68] substantial "self-therapeutic" (anticancer) properties of the unfunctionalized (i.e., not carrying cytotoxic payload) base C' dot,[51,63,65] a high drug loading capacity despite their ultrasmall particle size,[58,59] and a wide therapeutic index.[60] Furthermore, our results may also generate renewed interest in future studies on the connection between silica-containing nutritional products and their safety and potential health benefits.

Supporting Information

Supporting Information is available from the Wiley Online Library or from the author.

Acknowledgements

J.A.E., N.B., and T.C.G. equally contributed to this work. J.A.E., N.B., T.C.G., and U.B.W. designed the experiments. J.A.E., T.C.G., F.F.K, T.K., K.M., M.Z.T, R.L., N.N., and J.F.T. synthesized all nanoparticles used in this study. J.A.E., T.C.G, and F.F.K. performed confocal FCS and UV–vis spectroscopy. T.C.G., W.L.M., D.V.C., and T.A. performed TEM. T.C.G. and N.D. performed mucus reconstitution and rheological investigations. L.T. performed zeta potential experiments. N.B. and T.C.G. performed imaging FCS experiments. J.A.E., G.B.F., and N.N. did cell culturing and performed Caco-2 cell experiments. S.D.B. performed oral gavage, urine collection, and care for mice. J.A.E. performed analysis on urine samples. J.A.E., T.C.G., N.D., and H.F.M. formed pills and performed dissolution experiments. J.A.E., N.B., T.C.G., and U.B.W. analyzed and interpreted data and wrote the manuscript. All authors approved the final version of the manuscript. The authors would like to gratefully acknowledge David Putnam for helpful discussions. Mouse absorption studies were done via the Progressive Assessment of Therapeutics (PATh) core facility. This work

was funded by the National Cancer Institute of the National Institutes of Health under Award Number U54CA199081. Imaging data was acquired through the Cornell Institute of Biotechnology's Imaging Facility, with NIH S10OD025049 for the IVIS Spectrum. Imaging data was acquired through the Cornell Institute of Biotechnology's Imaging Facility, with NIH 1S10RR025502 funding for the shared Zeiss LSM 710 Confocal Microscope. TEM was performed at the Cornell Center for Materials Research (NSF MRSEC program under DMR-1719875) and funded by the Department of Energy (DE-SC0010560).

Conflict of Interest

A patent disclosure has been submitted to Cornell's Center for Technology Licensing. U.B.W. is a co-founder and sits on the Board of Directors of Elucida Oncology, Inc., which has licensed IP on C' dots coming out of the Wiesner Group at Cornell from Cornell University. J.A.E., T.C.G., and M.Z.T. are employees of Elucida. S.M. has no COI with the work reported in this paper; in the interest of full disclosure, he is a co-founder and sits on the Board of Directors of CitaScan, which is commercializing point-of-care technology for nutritional status partially developed in his lab at Cornell University.

Data Availability Statement

The data that support the findings of this study are available from the corresponding author upon reasonable request.

Keywords

Caco-2 permeability, imaging fluorescence correlation spectroscopy, mucus diffusion, nanoparticle oral delivery, nanoparticle pill formulation

Received: June 19, 2023
Revised: September 7, 2023
Published online: November 23, 2023

[1] S. Mitragotri, P. A. Burke, R. Langer, *Nat. Rev. Drug Discovery* **2014**, *13*, 655.
[2] A. C. Anselmo, Y. Gokarn, S. Mitragotri, *Nat. Rev. Drug Discovery* **2018**, *18*, 19.
[3] A. M. Vargason, A. C. Anselmo, S. Mitragotri, *Nat. Biomed. Eng.* **2021**, *5*, 951.
[4] M. May, *Nat. Med.* **2022**, *28*, 1100.
[5] J. M. Cyriac, E. James, *J. Pharmacol. Pharmacother.* **2014**, *5*, 83.
[6] F. Sevinc, J. M. Prins, R. P. Koopmans, P. N. J. Langendijk, P. M. Bossuyt, J. Dankert, P. Speelman, *J. Antimicrob. Chemother.* **1999**, *43*, 601.
[7] C. M. Hartshorn, M. S. Bradbury, G. M. Lanza, A. E. Nel, J. Rao, A. Z. Wang, U. B. Wiesner, L. Yang, P. Grodzinski, *ACS Nano* **2018**, *12*, 24.
[8] D. A. Scheinberg, J. Grimm, D. A. Heller, E. P. Stater, M. Bradbury, M. R. Mcdevitt, *Curr. Opin. Biotechnol.* **2017**, *46*, 66.
[9] A. Schroeder, D. A. Heller, M. M. Winslow, J. E. Dahlman, G. W. Pratt, R. Langer, T. Jacks, D. G. Anderson, *Nat. Rev. Cancer* **2012**, *12*, 39.
[10] W. R. Sanhai, J. H. Sakamoto, R. Canady, M. Ferrari, *Nat. Nanotechnol.* **2008**, *3*, 242.
[11] V. Wagner, A. Dullaart, A.-K. Bock, A. Zweck, *Nat. Biotechnol.* **2006**, *24*, 1211.
[12] A. A. Date, J. Hanes, L. M. Ensign, *J. Controlled Release* **2016**, *240*, 504.
[13] B. Homayun, X. Lin, H.-J. Choi, *Pharmaceutics* **2019**, *11*, 129.
[14] M. Herath, S. Hosie, J. C. Bornstein, A. E. Franks, E. L. Hill-Yardin, *Front. Cell. Infect. Microbiol.* **2020**, *10*, 248.
[15] A. Macierzanka, A. R. Mackie, L. Krupa, *Sci. Rep.* **2019**, *9*, 17516.
[16] J. Leal, H. D. C. Smyth, D. Ghosh, *Int. J. Pharm.* **2017**, *532*, 555.
[17] J. Witten, T. Samad, K. Ribbeck, *Curr. Opin. Biotechnol.* **2018**, *52*, 124.
[18] R. A. Cone, *Adv. Drug Delivery Rev.* **2009**, *61*, 75.
[19] S. K. Lai, Y.-Y. Wang, J. Hanes, *Adv. Drug Delivery Rev.* **2009**, *61*, 158.
[20] M. Yu, L. Xu, F. Tian, Q. Su, N. Zheng, Y. Yang, J. Wang, A. Wang, C. Zhu, S. Guo, X. X. Zhang, Y. Gan, X. Shi, H. Gao, *Nat. Commun.* **2018**, *9*, 1869.
[21] W. Shan, Xi Zhu, M. Liu, L. Li, J. Zhong, W. Sun, Z. Zhang, Y. Huang, *ACS Nano* **2015**, *9*, 2345.
[22] S. K. Lai, D. E O'hanlon, S. Harrold, S. T. Man, Y.-Y. Wang, R. Cone, J. Hanes, *Proc. Natl. Acad. Sci. U. S. A.* **2007**, *104*, 1482.
[23] B. Du, M. Yu, J. Zheng, *Nat. Rev. Mater.* **2018**, *3*, 358.
[24] A. A. Burns, J. Vider, H. Ow, E. Herz, O. Penate-Medina, M. Baumgart, S. M. Larson, U. Wiesner, M. Bradbury, *Nano Lett.* **2009**, *9*, 442.
[25] E. Phillips, O. Penate-Medina, P. B. Zanzonico, R. D. Carvajal, P. Mohan, Y. Ye, J. Humm, M. Gönen, H. Kalaigian, H. Schöder, H. W Strauss, S. M. Larson, U. Wiesner, M. S. Bradbury, *Sci. Transl. Med.* **2014**, *6*, 260ra149.
[26] F. Chen, K. Ma, B. Madajewski, L. Zhuang, L. Zhang, K. Rickert, M. Marelli, B. Yoo, M Z. Turker, M. Overholtzer, T. P. Quinn, M. Gonen, P. Zanzonico, A. Tuesca, M. A. Bowen, L. Norton, J. A Subramony, U. Wiesner, M. S. Bradbury, *Nat. Commun.* **2018**, *9*, 4141.
[27] H. Soo Choi, W. Liu, P. Misra, E. Tanaka, J. P. Zimmer, B. Itty Ipe, M. G. Bawendi, J. V. Frangioni, *Nat. Biotechnol.* **2007**, *25*, 1165.
[28] X. Yang, K. Forier, L. Steukers, S. Van Vlierberghe, P. Dubruel, K. Braeckmans, S. Glorieux, H. J. Nauwynck, *PLoS One* **2012**, *7*, 51054.
[29] N. Chenouard, I. Smal, F. De Chaumont, M. Maska, I. F. Sbalzarini, Y. Gong, J. Cardinale, C. Carthel, S. Coraluppi, M. Winter, A. R. Cohen, W. J. Godinez, K. Rohr, Y. Kalaidzidis, L. Liang, J. Duncan, H. Shen, Y. Xu, K. E. G. Magnusson, J. Jaldén, H. M. Blau, P. Paul-Gilloteaux, P. Roudot, C. Kervrann, F. Waharte, J.-Y. Tinevez, S. L. Shorte, J. Willemse, K. Celler, G. P. Van Wezel, et al., *Nat. Methods* **2014**, *11*, 281.
[30] J. S. Suk, S. K. Lai, Y.-Y. Wang, L. M. Ensign, P. L. Zeitlin, M. P. Boyle, J. Hanes, *Biomaterials* **2009**, *30*, 2591.
[31] B. S. Schuster, J. S. Suk, G. F. Woodworth, J. Hanes, *Biomaterials* **2013**, *34*, 3439.
[32] C. S. Schneider, Q. Xu, N. J. Boylan, J. Chisholm, B. C. Tang, B. S. Schuster, A. Henning, L. M. Ensign, E. Lee, P. Adstamongkonkul, B. W. Simons, S-Yu S. Wang, X. Gong, T. Yu, M. P. Boyle, J. S. Suk, J. Hanes, *Sci. Adv.* **2017**, *3*, 1601556.
[33] V. Snoeck, B. Goddeeris, E. Cox, *Microbes Infect.* **2005**, *7*, 997.
[34] P. Lundquist, P. Artursson, *Adv. Drug Delivery Rev.* **2016**, *106*, 256.
[35] P. Artursson, J. Karlsson, *Biochem. Biophys. Res. Commun.* **1991**, *175*, 880.
[36] P. Artursson, K. Palm, K. Luthman, *Adv. Drug Delivery Rev.* **2001**, *46*, 27.
[37] M. Pinto, S. Robine Leon, M. D. Appay, *Biol. Cell.* **1983**, *47*, 323.
[38] Y. Sambuy, I. De Angelis, G. Ranaldi, M. L. Scarino, A. Stammati, F. Zucco, *Cell Biol. Toxicol.* **2005**, *21*, 1.
[39] I. Hubatsch, E. G. E. Ragnarsson, P. Artursson, *Nat. Protoc.* **2007**, *2*, 2111.
[40] A. Banerjee, J. Qi, R. Gogoi, J. Wong, S. Mitragotri, *J. Controlled Release* **2016**, *238*, 176.
[41] J. Garcia-Fernandez, D. Turiel, J. Bettmer, N. Jakubowski, U. Panne, L. Rivas García, J. Llopis, C. Sánchez González, M. Montes-Bayón, *Nanotoxicology* **2020**, *14*, 388.
[42] A. Alalaiwe, G. Roberts, P. Carpinone, J. Munson, S. Roberts, *Drug Delivery* **2017**, *24*, 591.

[43] S. Zhu, X. Jiang, M. D. Boudreau, G. Feng, Y. Miao, S. Dong, H. Wu, M. Zeng, J.-J. Yin, *J. Nanobiotechnol.* **2018**, *16*, 86.
[44] R. Cornu, C. Chrétien, Y. Pellequer, H. Martin, A. Béduneau, *Arch. Toxicol.* **2020**, *94*, 1191.
[45] D. Ye, M. Bramini, D. R. Hristov, S. Wan, A. Salvati, C. Åberg, K. A. Dawson, *Beilstein J. Nanotechnol.* **2017**, *8*, 1396.
[46] N. G. Lamson, A. Berger, K. C. Fein, K. A. Whitehead, *Nat. Biomed. Eng.* **2020**, *4*, 84.
[47] Y. Zhang, M. Xiong, X. Ni, J. Wang, H. Rong, Y. Su, S. Yu, I. S. Mohammad, S. S. Y. Leung, H. Hu, *ACS Appl. Mater. Interfaces* **2021**, *13*, 18077.
[48] Y. Gao, Y. He, H. Zhang, Y. Zhang, T. Gao, J.-H. Wang, S. Wang, *J. Colloid Interface Sci.* **2021**, *582*, 364.
[49] X. Tan, X. Liu, Y. Zhang, H. Zhang, X. Lin, C. Pu, J. Gou, H. He, T. Yin, Y. Zhang, X. Tang, *Expert Opin. Drug Delivery* **2018**, *15*, 805.
[50] K. Ma, C. Mendoza, M. Hanson, U. Werner-Zwanziger, J. Zwanziger, U. Wiesner, *Chem. Mater.* **2015**, *27*, 4119.
[51] S. E. Kim, L. Zhang, K. Ma, M. Riegman, F. Chen, I. Ingold, M. Conrad, M. Z. Turker, M. Gao, X. Jiang, S. Monette, M. Pauliah, M. Gonen, P. Zanzonico, T. Quinn, U. Wiesner, M. S. Bradbury, M. Overholtzer, *Nat. Nanotechnol.* **2016**, *11*, 977.
[52] F. Chen, B. Madajewski, K. Ma, D. Karassawa Zanoni, H. Stambuk, M. Z. Turker, S. Monette, L. Zhang, B. Yoo, P. Chen, R. J. C. Meester, S De Jonge, P. Montero, E. Phillips, T. P. Quinn, M. Gönen, S. Sequeira, E. De Stanchina, P. Zanzonico, U. Wiesner, S. G. Patel, M. S. Bradbury, *Sci. Adv.* **2019**, *5*, aax5208.
[53] K. P. Barteau, K. Ma, F. F. E. Kohle, T. C. Gardinier, P. A. Beaucage, R. E. Gillilan, U. Wiesner, *Chem. Mater.* **2019**, *31*, 643.
[54] K. Ma, D. Zhang, Y. Cong, U. Wiesner, *Chem. Mater.* **2016**, *28*, 1537.
[55] T. C. Gardinier, F. F. E. Kohle, J. S. Peerless, K. Ma, M. Z. Turker, J. A. Hinckley, Y. G. Yingling, U. Wiesner, *ACS Nano* **2019**, *13*, 1795.
[56] T. C. Gardinier, M. Z. Turker, J. A. Hinckley, W. P. Katt, N. Domnwachukwu, F. Woodruff, J. Hersh, J. Wang, R. A. Cerione, U. B. Wiesner, *J. Phys. Chem. C* **2019**, *123*, 23246.
[57] K. Ma, U. Wiesner, *Chem. Mater.* **2017**, *29*, 6840.
[58] F. Wu, T. C. Gardinier, M. Z. Turker, F. Chen, P.-M. Chen, A. M. Venkatesan, V. Patel, G. P. Adams, M. S. Bradbury, U. B. Wiesner, G. Germano, K. Ma, *Chem. Mater.* **2022**, *34*, 5344.
[59] F. Wu, P.-M. Chen, T. C. Gardinier, M. Z. Turker, A. M. Venkatesan, V. Patel, T. Khor, M. S. Bradbury, U. B. Wiesner, G. P. Adams, G. Germano, F. Chen, K. Ma, *ACS Nano* **2022**, *16*, 20021.
[60] L. Zhang, V. Aragon-Sanabria, A. Aditya, M. Marelli, T. Cao, F. Chen, B. Yoo, K. Ma, L. Zhuang, T. Cailleau, L. Masterson, M. Z. Turker, R. Lee, G. Deleon, S. Monette, R. Colombo, R. J. Christie, P. Zanzonico, U. Wiesner, J. A Subramony, M. S. Bradbury, *Adv. Ther.* **2023**, *6*, 2200209.
[61] B. Madajewski, F. Chen, B. Yoo, M. Z. Turker, K. Ma, L. Zhang, P.-M. Chen, R. Juthani, V. Aragon-Sanabria, M. Gonen, C. M. Rudin, U. Wiesner, M. S. Bradbury, C. Brennan, *Clin. Cancer Res.* **2020**, *26*, 5424.
[62] F. Chen, K. Ma, L. Zhang, B. Madajewski, P. Zanzonico, S. Sequeira, M. Gonen, U. Wiesner, M. S. Bradbury, *Chem. Mater.* **2017**, *29*, 8269.
[63] M. Riegman, L. Sagie, C. Galed, T. Levin, N. Steinberg, S. J. Dixon, U. Wiesner, M. S. Bradbury, P. Niethammer, A. Zaritsky, M. Overholtzer, *Nat. Cell Biol.* **2020**, *22*, 1042.
[64] W. Wang, M. Green, J. E. Choi, M. Gijón, P. D. Kennedy, J. K. Johnson, P. Liao, X. Lang, I. Kryczek, A. Sell, H. Xia, J. Zhou, G. Li, J. Li, W. Li, S. Wei, L. Vatan, H. Zhang, W. Szeliga, W. Gu, R. Liu, T. S. Lawrence, C. Lamb, Y. Tanno, M. Cieslik, E. Stone, G. Georgiou, T. A. Chan, A. Chinnaiyan, W. Zou, *Nature* **2019**, *569*, 270.
[65] A. M. Urbanska, R. Khanin, S. Alidori, S. Wong, B. P. Mello, B. A. Almeida, F. Chen, K. Ma, M. Z. Turker, T. Korontsvit, D. A. Scheinberg, P. B. Zanzonico, U. Wiesner, M. S. Bradbury, T. P. Quinn, M. R. McDevitt, *Cancer Biother. Radiopharm.* **2020**, *35*, 459.
[66] N. Bag, T. Wohland, *Annu. Rev. Phys. Chem.* **2014**, *65*, 225.
[67] H. Mohammad-Beigi, Y. Hayashi, C. M. Zeuthen, H. Eskandari, C. Scavenius, K. Juul-Madsen, T. Vorup-Jensen, J. J. Enghild, D. S. Sutherland, *Nat. Commun.* **2020**, *11*, 4535.
[68] D. K. Zanoni, H. E. Stambuk, B. Madajewski, P. H. Montero, D. Matsuura, K. J. Busam, K. Ma, M. Z. Turker, S. Sequeira, M. Gonen, P. Zanzonico, U. Wiesner, M. S. Bradbury, S. G. Patel, *JAMA Network Open* **2021**, *4*, 211936.
[69] T. Kao, F. Kohle, K. Ma, T. Aubert, A. Andrievsky, U. Wiesner, *Nano Lett.* **2018**, *18*, 1305.
[70] K. D. Hartlen, A. P. T. Athanasopoulos, V. Kitaev, *Langmuir* **2008**, *24*, 1714.
[71] T. Yokoi, Y. Sakamoto, O. Terasaki, Y. Kubota, T. Okubo, T. Tatsumi, *J. Am. Chem. Soc.* **2006**, *128*, 13664.
[72] D. R. Larson, H. Ow, H. D. Vishwasrao, A. A. Heikal, U. Wiesner, W. W. Webb, *Chem. Mater.* **2008**, *20*, 2677.
[73] F. F. E. Kohle, J. A. Hinckley, U. B. Wiesner, *J. Phys. Chem. C* **2019**, *123*, 9813.
[74] J. David Friedl, V. Nele, G. De Rosa, A. Bernkop-Schnürch, J. D. Friedl, A. Bernkop-Schnürch, V. Nele, G. De Rosa, *Adv. Funct. Mater.* **2021**, *31*, 2103347.
[75] J.-M. Rabanel, P. Hildgen, X. Banquy, *J. Controlled Release* **2014**, *185*, 71.
[76] Y.-Y. Wang, S. K. Lai, J. S. Suk, A. Pace, R. Cone, J. Hanes, *Angew. Chem., Int. Ed.* **2008**, *47*, 9726.
[77] J. T. Huckaby, S. K. Lai, *Adv. Drug Delivery Rev.* **2018**, *124*, 125.
[78] J. A. Lee, M. K. Kim, H. J. Paek, Y. R. Kim, M. K. Kim, J. K. Lee, J. Jeong, S. J. Choi, *Int. J. Nanomed.* **2014**, *9*, 251.
[79] J. A. Caicedo, J. E. Perilla, *Ing. Invest.* **2015**, *35*, 43.
[80] D. Walker, B. T. Käsdorf, H.-H. Jeong, O. Lieleg, P. Fischer, *Sci. Adv.* **2015**, *1*, 1500501.
[81] L. A. Sellers, A. Allen, E. R. Morris, S. B. Ross-Murphy, *Biochim. Biophys. Acta, Gen. Subj.* **1991**, *1115*, 174.
[82] L. A. Sellers, A. Allen, E. R. Morris, S. B. Ross-Murphy, *Biorheology* **1987**, *24*, 615.
[83] S. K. Lai, Y.-Y. Wang, D. Wirtz, J. Hanes, *Adv. Drug Delivery Rev.* **2009**, *61*, 86.
[84] M. Liu, J. Zhang, W. Shan, Y. Huang, *Asian J. Pharm. Sci.* **2015**, *10*, 275.
[85] S. Zustiak, J. Riley, H. Boukari, A. Gandjbakhche, R. Nossal, *J. Biomed. Opt.* **2012**, *17*, 125004.
[86] B. Kannan, L. Guo, T. Sudhaharan, S. Ahmed, I. Maruyama, T. Wohland, *Anal. Chem.* **2007**, *79*, 4463.
[87] J. Sankaran, M. Manna, L. Guo, R. Kraut, T. Wohland, *Biophys. J.* **2009**, *97*, 2630.
[88] S. J. Lord, H.-Lu D. Lee, W. E. Moerner, *Anal. Chem.* **2010**, *82*, 2192.
[89] D. Wang, A. Agrawal, R. Piestun, D. K. Schwartz, *Appl. Phys. Lett.* **2017**, *110*, 211107.
[90] M. Tokunaga, N. Imamoto, K. Sakata-Sogawa, *Nat. Methods* **2008**, *5*, 159.
[91] C. A. Konopka, S. Y. Bednarek, *Plant J.* **2008**, *53*, 186.
[92] J. Sankaran, X. Shi, L. Y. Ho, E. H. K. Stelzer, T. Wohland, *Opt. Express* **2010**, *18*, 25468.
[93] M. J. Santander-Ortega, M. Plaza-Oliver, V. Rodríguez-Robledo, L. Castro-Vázquez, N. Villaseca-González, J. González-Fuentes, E. L. Cano, P. Marcos, M. V. Lozano, M. M. Arroyo-Jiménez, *Langmuir* **2017**, *33*, 4269.
[94] W. Sumsakul, K. Na-Bangchang, *Arch. Pharm. Res.* **2016**, *39*, 380.
[95] V. C. Ude, D. M. Brown, L. Viale, N. Kanase, V. Stone, H. J. Johnston, *Part. Fibre Toxicol.* **2017**, *14*, 31.
[96] J. A. Erstling, J. A. Hinckley, N. Bag, J. Hersh, G. B. Feuer, R. Lee, H. F. Malarkey, F. Yu, K. Ma, B. A. Baird, U. B. Wiesner, *Adv. Mater.* **2021**, *33*, 2006829.

[97] R. Lee, J. A. Erstling, J. A. Hinckley, D. V. Chapman, U. B. Wiesner, *Adv. Funct. Mater.* **2021**, *31*, 2106144.
[98] R. K. Iler, *The Chemistry of Silica: Solubility, Polymerization, Colloid and Surface Properties and Biochemistry of Silica*, John Wiley & Sons, New York **1979**.
[99] R. Schwarz, A. Kaspar, J. Seelig, B. Künnecke, *Magn. Reson. Med.* **2002**, *48*, 255.
[100] E. L. Mcconnell, A. W. Basit, S. Murdan, *J. Pharm. Pharmacol.* **2008**, *60*, 63.
[101] Y. Qian, J. Zhang, X. Fu, R. Yi, P. Sun, M. Zou, X. Long, X. Zhao, *Molecules* **2018**, *23*, 2848.
[102] W. Yan, Z. Zhang, X. Guo, W. Liu, Z. Song, *ECS J. Solid State Sci. Technol.* **2015**, *4*, P108.
[103] C. H. C. Leenaars, C. Kouwenaar, F. R. Stafleu, A. Bleich, M. Ritskes-Hoitinga, R. B. M. De Vries, F. L. B. Meijboom, *J. Transl. Med.* **2019**, *17*, 223.
[104] H. Musther, A. Olivares-Morales, O. J. D. Hatley, B. Liu, A. Rostami Hodjegan, *Eur. J. Pharm. Sci.* **2014**, *57*, 280.
[105] D. Magde, E. L. Elson, W. W. Webb, *Biopolymers* **1974**, *13*, 29.
[106] B. A. Inman, W. Etienne, R. Rubin, R. A. Owusu, T R. Oliveira, D. B. Rodriques, P. F. Maccarini, P. R. Stauffer, A. Mashal, M. W. Dewhirst, *Int. J. Hyperthermia* **2013**, *29*, 206.
[107] R. Burton-Opitz, R. Dinegar, *Am. J. Physiol.* **1918**, *47*, 220.
[108] C. C. M. C. Carcouët, M. W. P. Van De Put, B. Mezari, P. C. M. M. Magusin, J. Laven, P. H. H. Bomans, H. Friedrich, A. C. C. Esteves, N. A. J. M. Sommerdijk, R. A. T. M. Van Benthem, G. De With, *Nano Lett.* **2014**, *14*, 1433.
[109] M. Sumper, N. Kröger, *J. Mater. Chem.* **2004**, *14*, 2059.
[110] J. L. Finkelstein, S. Colt, A. J. Layden, J. T. Krisher, A. M. Stewart-Ibarra, M. Polhemus, E. Beltrán-Ayala, J. M. Tedesco, W. B. Cárdenas, T. Endy, S. Mehta, *J. Infect. Dis.* **2020**, *221*, 91.
[111] K. R. Martin, *J. Nutr.* **2007**, *11*, 94.
[112] S. Gillette-Guyonnet, S. Andrieu, B. Vellas, *J. Nutr.* **2007**, *11*, 119.
[113] W. Y. Wu, P. L. Chou, J. C. Yang, C. T. Chien, *PLoS One* **2021**, 16.
[114] H. C. Winkler, M. Suter, H. Naegeli, *J Nanobiotechnol.* **2016**, *14*, 44.